

# Cardiac Magnetic Resonance Elastography

## Initial Results

Thomas Elgeti, MD,\* Jens Rump, MS,\* Uwe Hamhaber, PhD,† Sebastian Papazoglou, MS,\*  
Bernd Hamm, MD,\* Jürgen Braun, PhD,† and Ingolf Sack, PhD\*

**Objectives:** To develop cardiac magnetic resonance elastography (MRE) for noninvasively measuring left ventricular (LV) pressure-volume (P-V) work.

**Material and Methods:** The anterior chest wall of 8 healthy volunteers was vibrated by 24.3-Hz acoustic waves for stimulating oscillating shear deformation in myocardium and adjacent blood. The induced motion was recorded by an electrocardiogram-gated, vibration-synchronized and segmented gradient-recalled echo MRE sequence acquiring 360 phase-contrast wave images with a temporal resolution of 5.16 milliseconds in the short-axis view during controlled breathing. Relative changes in wave amplitudes served as a measure of LV pressure variation during the cardiac cycle. MRE pressure data were combined with LV volumes obtained from segmentation of 3D cine-steady-state free precession data sets.

**Results:** Shear wave amplitudes decreased from diastole to systole, which reflects the dynamics of myocardial shear modulus variations during the cardiac cycle. Assuming spherical shear stress, a linear relationship between myocardial stiffness and LV pressure was derived. The MRE-measured pressure was plotted as a function of LV volumes. Characteristic P-V cycles displayed an isovolumetric increase in pressure during early systole, whereas less pronounced volume conservation was observed in early diastole. Mean cardiac P-V work in all volunteers was  $0.85 \pm 0.11$  J.

**Conclusion:** In vivo cardiac MRE is a noninvasive method for measuring pressure-related heart function determined by shear modulus variations in the LV wall. This is the first noninvasive mechanical test of cardiac work in the human heart and is potentially useful for assessing pathologies associated with increased myocardial stiffness such as diastolic dysfunction.

**Key Words:** MR elastography, cardiac function, shear modulus, pressure, volume

(*Invest Radiol* 2008;43: 762–772)

Received January 21, 2008, and accepted for publication, after revision, May 30, 2008.

From the \*Department of Radiology, Charité-Universitätsmedizin Berlin, Campus Mitte, Berlin, Germany; and †Institute of Medical Informatics, Charité-Universitätsmedizin Berlin, Campus Benjamin Franklin, Berlin, Germany.

Supported by German Research Foundation (Sa/901-3).

Reprints: Ingolf Sack, PhD, Department of Radiology, Charité-Universitätsmedizin Berlin, Charitéplatz 1, 10117 Berlin, Germany. E-mail: ingolf.sack@charite.de

Copyright © 2008 by Lippincott Williams & Wilkins  
ISSN: 0020-9996/08/4311-0762

The pressure-volume (P-V) relationship is a highly reliable parameter for assessing myocardial contractility in the intact circulation. This relationship is almost insensitive to changes in preload and afterload, which is why it is widely used in animal studies and occasionally clinically.<sup>1,2</sup> Determination of the P-V relationship requires the simultaneous acquisition of ventricular volume and pressure data. While ventricular volume can be noninvasively assessed by modern imaging modalities, the gold standard for determining ventricular pressure continues to be measurements performed using high fidelity micromanometers or conductance catheters during cardiac catheterization.<sup>3,4</sup> The demanding technique and a relatively high probability of undesirable events during the invasive procedure limits its daily use, and consequently there is a lack of pertinent information for the diagnosis of heart diseases that are neither associated with a clear morphologic typology nor develop a characteristic motion, strain or perfusion pattern that can be visualized with echocardiography or magnetic resonance imaging (MRI).<sup>5–7</sup> Particularly the definition of diastolic dysfunction remains demanding since myocardial relaxation is most pronounced during left ventricular (LV)-inflow and ventricular pressure evolution. Different parameters have been proposed for non-invasively identifying diastolic dysfunction using echocardiography.<sup>8,9</sup> Widely used parameters are the mitral valve inflow pattern, isovolumetric relaxation (IVR) time and other parameters derived from tissue Doppler imaging. Despite the indisputable benefit of echocardiographic indices in modern cardiology, ventricular pressure or pressure-related quantities cannot be measured without applying forces to the heart. Furthermore, the hemodynamic counterforce or the response of the tissue to external or intrinsic mechanical stimulation has to be measured.<sup>4</sup>

### MR Elastography

Elastography combines mechanical tissue stimulation with the measurement of the resulting deformation using soft-tissue imaging modalities such as MRI or ultrasound for measuring shear waves.<sup>10,11</sup> The stimulated shear deformation measured by elastography is related to the shear-elastic and shear-viscous behavior of biologic tissues that varies by several orders of magnitude throughout the human body.<sup>12</sup> Recently, MR elastography (MRE) has shown rapid progress in the assessment of the viscoelastic behavior of human organs that are not palpable from the body surface.<sup>13–16</sup> In

MRE, vibrations are induced in an acoustic frequency range between 25 and 100 Hz and recorded by phase-contrast imaging techniques. The resulting shear wave images are traditionally analyzed by wave-inversion algorithms.<sup>17</sup> Although wave inversion principally allows the deduction of stiffness maps from wave patterns, its practical value strongly depends on a variety of experimental constraints that inherently impair the resolution of stiffness details.<sup>18</sup> Most importantly, viscous properties cause wave energy absorption and thus a fast obliteration of shear waves as a function of the excitation frequency.<sup>16,19</sup> For this reason, low-frequency vibrations able to sufficiently penetrate the human heart are associated with large wavelengths that are not amenable to wave-inversion analysis.

## Cardiac MR Elastography

In this study, we introduce a MRE method that is dedicated to myocardial shear modulus measurements in the intact human heart. The acquired stiffness data will be assigned to the ventricular pressure evolution during the heart cycle. To avoid confusion with invasive pressure curves in the literature,<sup>4</sup> the MRE-derived pressure will be denoted as  $p_{MRE}$  and is assumed to be the linear and instantaneous response to myocardial shear modulus variations  $\mu(t)$ . The following major developments were necessary to design a cardiac MRE technique capable of acquiring P-V data: (1) a mechanical driver was built that efficiently vibrates the chest by 25-Hz acoustic waves; (2) a motion-synchronized acquisition sequence was developed that yields time-resolved wave images with an image-frame rate of approximately 200 Hz; (3) signal cross-correlation was used for separating the oscillatory wave signal from intrinsic motions; and (4) theoretical models were derived for calculating MRE pressure data from wave amplitudes.

## MATERIALS AND METHODS

### From Shear Wave Amplitudes to Pressure

While traditional MRE relies on wave inversion, the technique introduced here is based on evaluating the variation of wave amplitudes  $U(t)$  during the cardiac cycle. In this approach, the variation of  $U(t)$  in a medium of temporally varying elasticity is attributed to the relative change in the shear modulus  $\mu(t)$  that holds for a constant wave intensity.<sup>20</sup> As shown further down, for harmonic shear waves, the ratio of  $U^4$  and  $\mu$  is the same at a different time point during the cardiac cycle. Thus, relative changes in wave amplitudes can be related to relative changes in the shear modulus. Similar to other muscle, the variation of the intrinsic shear modulus of the myocardium initiates myocardial shear strain and shear stress. Assuming a spherical LV geometry, the radial shear-stress component is in equilibrium with the internal cavity pressure.<sup>21</sup> In the appendix, a model is presented that describes the development of radial shear stress and cavity pressure from spherical shear deformations without compression. It is shown that the shear modulus is proportional to cavity pressure assuming a small and constant shear strain. This condition assumes an instantaneous pressure response to myocardial stiffness variations, ie, no large deformations

dilute the effect of the intrinsic shear modulus. Combined with elastic wave theory the spherical shear-stress model allows one to deduce a simple relation between shear wave amplitudes  $U(t)$  and pressure  $p_{MRE}(t)$  (see appendix):

$$p_{MRE}(t) = \left( \frac{U_{systole}}{U(t)} \right)^4 p_{systole} \quad (1)$$

$p_{systole}$  is the externally measured systolic blood pressure that is taken to be equivalent to end-systolic LV cavity pressure. Eq. 1 specifically applies to the isovolumetric contraction (IVC) and isovolumetric relaxation (IVR) of the myocardium during which only minor deformation occurs. Geometrical effects during other phases of the cardiac cycle are not considered and thus, the derived quantity is the MRE pressure  $p_{MRE}$ . In the following Eq. 1 is used to calculate  $p_{MRE}(t)$  from wave amplitudes  $U(t)$ .  $U(t)$  is determined in the left ventricle in 8 healthy volunteers within 1 R-R interval of the electrocardiogram (ECG). Cardiac MRE data are combined with 3D-MRI volumetry of the left ventricle to analyze MRE P-V functions.

### Volunteers

Eight (2 females) volunteers without any previous history of cardiac disease (aged 25, 35, 33, 37, 35, 32, 22, and 34), in the following numbered from 1 to 8, were examined. The investigation conforms with the principles outlined in the Declaration of Helsinki. Institutional review board approval was obtained, and informed consent was obtained from all subjects.

Blood pressure and heart rate were recorded prior, during, and after the examination using a commercially available device (Multigasmonitor 9500, Medrad Inc., Indianapolis, PA). In 2 volunteers (#1 and #2), the experiments were 3 times repeated in a 6-month period to obtain P-V-curves for different times, heart rates, and nutritional states.

### MRI LV-Volumetry

All imaging was performed on a 1.5 T scanner (Siemens Sonata, Erlangen, Germany) using a standard 12 element body phased-array coil. After piloting, retrospectively ECG-gated cine-steady-state free precession sequences were obtained in the doubly angulated 3 long cardiac axes (slice thickness 5 mm, typical field of view [FoV] 370 mm × 310 mm, time of repetition [TR] 46.5 milliseconds, echo time [TE] 1.6 milliseconds, and matrix 256 × 160), and in the LV short axis (slice thickness 10 mm, typical FoV 320 × 240 mm, TR 40.7 milliseconds, TE 1.3 milliseconds, and matrix 192 × 144, acceleration factor 2 [integrated parallel acquisition technique, GRAPPA]) to cover the whole left ventricle.

### Cardiac MRE Experiments

Technical details of cardiac MRE are described in Ref.<sup>22</sup> In the following, important sequence parameter and the driver setup are briefly reviewed. A remote oscillator<sup>23</sup> was used to vibrate the chest of the volunteer (Fig. 1). A 2.5–3.0 m long transducer piston was mounted in the center of a loudspeaker membrane while the proximal end was positioned in the center of the volunteer's chest inside the

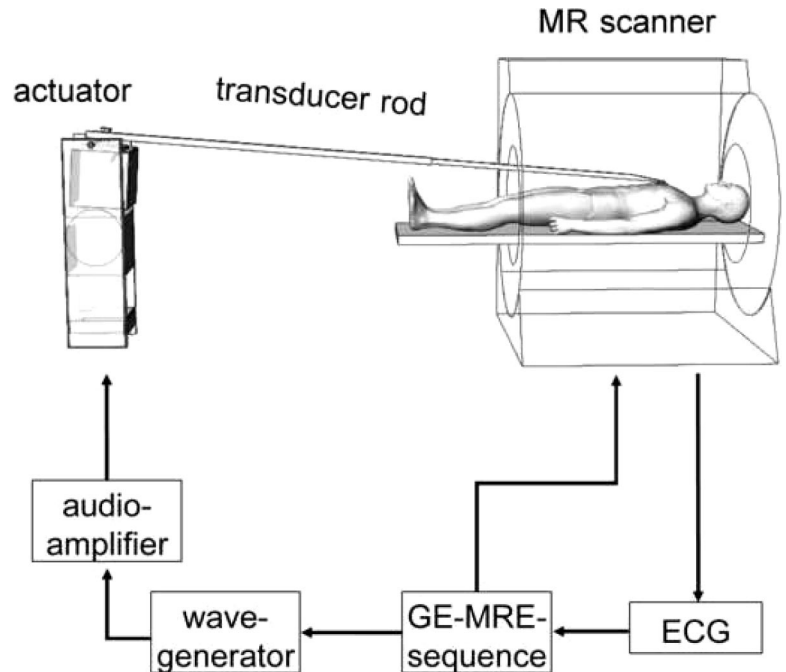


**FIGURE 1.** Flow chart of the trigger succession in cardiac MRE: The volunteer's ECG starts the MRE-sequence which causes the start of the wave generation (frequency 24.3 Hz) via wave-generator, audio-amplifier, actuator and transducer-rod onto the volunteer's chest.

scanner and kept in place solely by its own weight (approximately 1.5 kg). The R-wave of the ECG triggered the start of the MRE sequence that was synchronized to the vibration. The wave generator produced one sinusoidal burst of 41.28 milliseconds length (equal to 24.3 Hz driving frequency) after each eighth TR, which was amplified and fed into the actuator (Fig. 1).

An ECG-gated, gradient-recalled echo steady-state imaging sequence (TR 5.16 milliseconds, TE 1.3 milliseconds,  $\alpha = 15^\circ$ , RF spoiling, 2-fold GRAPPA acceleration, interpolation of k-space data from 64 phase-encoded lines to a  $128 \times 128$  matrix, typical FoV  $320 \times 250$  mm, 5 mm slice thickness, 34 k-space segments with one line per segment, single-cycle motion encoding gradient: 2 milliseconds duration, 35 mT/m amplitude in the read-out [RO] direction, 25 mT/m amplitude in the direction of phase-encoding [PE] or slice-selection [SS], steady-state conditions were reached after 20 TRs before the acquisition). Depending on the heart rate, the total acquisition time of approximately 2.5 minutes for each spatial direction of motion encoding results from 34 repetitive scans of 1.9608 seconds duration each ( $[360 + 20 \text{ transient TR's}] \times 5.16 \text{ milliseconds}$ ). Each of these scans was performed during breath-hold at end-expiration followed by a short delay of approximately 2.5 seconds for respiration. One reference experiment with SS-motion encoding gradient without vibration was followed by 3 vibration experiments with consecutive motion sensitization in SS, RO, and PE direction.

### LV Volume Analysis

LV volume-time curves were obtained by manually segmenting the LV endocardial contours over the cardiac cycle (25 reconstructed images, resulting in a temporal resolution of 40.7 milliseconds) in all short cardiac axes (10–13

different slice positions). Enddiastolic volume was defined as maximum volume of the left ventricle and endsystolic volume was the volume when the left ventricle was smallest. The epicardial contours were drawn in end-diastole for calculation of LV myocardial mass. Global LV ejection fraction was calculated as the ratio of stroke volume to enddiastolic volume. Commercially available software (ARGUS, Version Syngo MR 2004A, Siemens, Erlangen, Germany) was used. Volumes and myocardial mass were normalized to body surface area (BSA).

### MRE Data Processing

Image postprocessing was performed using custom-made software run on MATLAB (Version 7.0.4, The Math-Work Inc.). Blood flow and intrinsic cardiac motion were eliminated from the oscillatory signal as follows: first, calculation of the time derivate of the phase images ( $n = 360$ ) was combined with phase unwrapping. As a result, filtered flow data images were obtained showing a first suppression of the low-frequency components of cardiac motion. Second, the filtered images were subjected to signal cross-correlation using a complex, single-period sinusoid of the same length as the wave generator output. As each vibration cycle was sampled by 8 images, the resulting wave amplitude images ( $n = 45$ ) had an 8-fold lower temporal resolution than the oscillation data. Finally, the amplitude data were combined to calculate 1 R-R interval represented in 25  $U(x, y, t)$  images. The outer systolic contour of the left ventricle was manually segmented by means of the magnitude images of the MRE experiment. A region of interest (ROI) was then automatically placed within the systolic LV contour enclosing the region where  $U_{diastole} > U_{systole}$ . The endocardial contour of the ventricle was neglected as the change in wave amplitude of the blood near the myocardial wall reflects the change in

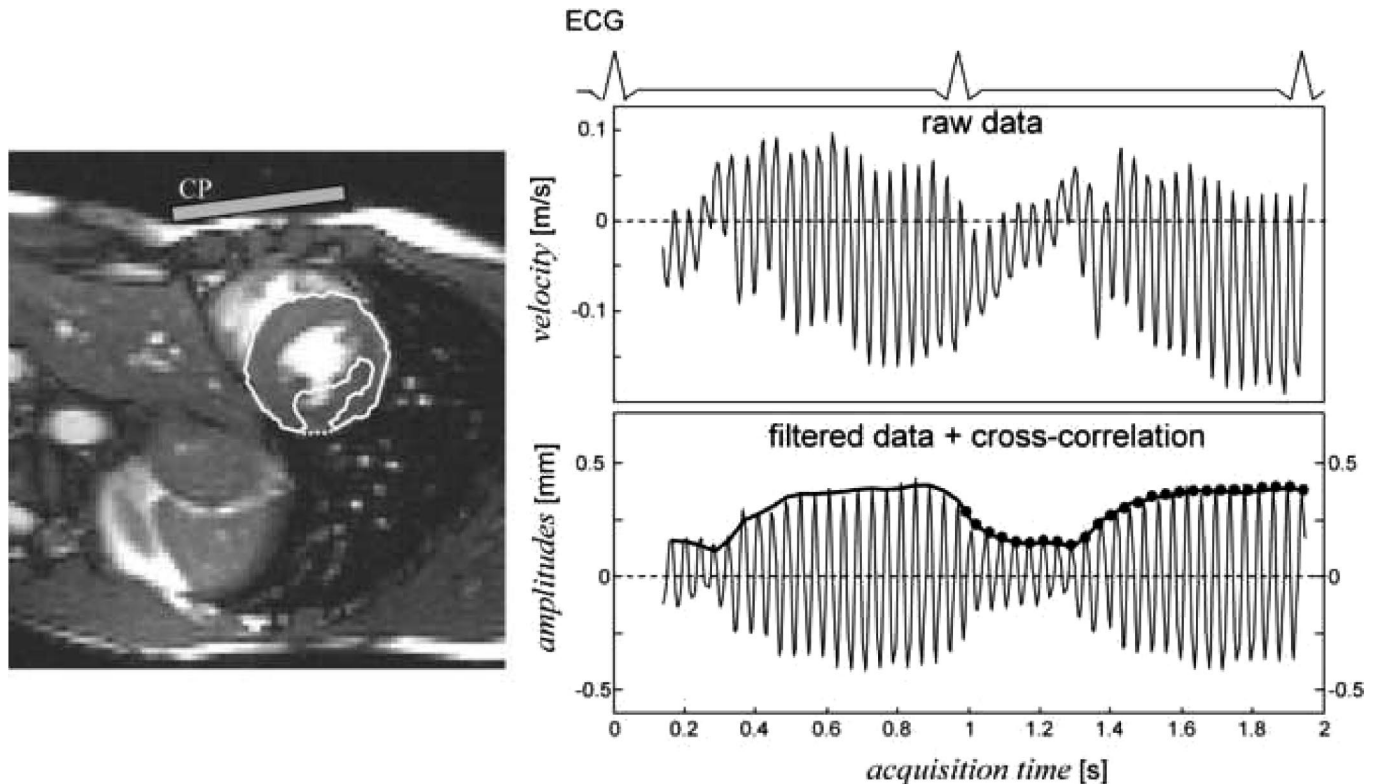


**FIGURE 2.** Schematic representation of the processing of oscillation-data in cardiac MRE. On the left-hand side a short cardiac axis with the connection plate (CP) on the anterior chest wall is shown. The region-of-interest (ROI, white line) is displayed used for spatial signal averaging of the oscillations plotted on the right-hand side against time. The ROI was derived by manual segmentation of the LV-epicardium (dotted white line) followed by an automatic refinement based on the wave amplitude variation  $U_{diastole}/U_{systole}$  (solid white line). The raw phase data display the left-to-right component of the superposition of blood flow, heart motion and wave oscillations. Linear filtering suppresses slow intrinsic motion components as shown below. The wave amplitudes are obtained after complex cross-correlation of the filtered oscillation data (fat line). The final wave amplitude data  $U(t)$  (solid circles) are combined to one R-R-interval.

myocardial elasticity due to boundary and surface effects<sup>20,24</sup> (Fig. 2). The wave amplitudes of each encoding direction (SS, RO, and PE) were spatially averaged within the ROI and combined by  $U = \sqrt{U_{SS}^2 + U_{RO}^2 + U_{PE}^2}$ . The registered systolic blood pressure was used as an estimate of maximum ventricular pressure  $p_{systole}$  for calculating  $p_{MRE}(t)$  by Eq. 1. From the resulting P-V data, the systolic and diastolic isopressure levels  $\bar{p}_{systole}$  and  $\bar{p}_{diastole}$  were determined by averaging 4 and 6 data points of minimum and maximum pressure, respectively. The intercepts of  $\bar{p}_{systole}$  and  $\bar{p}_{diastole}$  with the P-V graph were used to calculate the volume difference  $\Delta V$  during IVC and IVR. Then  $p'_{IVC}$  and  $p'_{IVR}$  were derived by  $(\bar{p}_{systole} - \bar{p}_{diastole})/\Delta V$  as a parameterization of the extent of volume conservation during IVC and IVR pressure changes.

### Statistics

All data are given as mean  $\pm$  SD. In this feasibility study, no dedicated statistical methods are used because only 8 subjects were investigated and there is considerable physiological fluctuation in the parameters measured, which cannot be controlled in such a small group of volunteers.

## RESULTS

The mean blood pressure measured was  $121/67 \pm 10/6$  mm Hg. The mean heart rate was  $64 \pm 9$  bpm.

### MRI

Global LV systolic function was normal in all volunteers (ejection fraction [EF]  $58 \pm 3.4\%$ ; range, 50–61%). Enddiastolic (EDV) and endsystolic (ESV) volumes were in the normal range (EDV normalized to BSA  $74.4 \pm 5.9$  mL/cm<sup>2</sup>, myocardial mass normalized to BSA  $58.6 \pm 3.5$  g/cm<sup>2</sup>).<sup>25</sup> One volunteer showed turbulent systolic flow in the left atrium, which was normal in size. In this volunteer (#3), mild mitral valve insufficiency (grade I) was confirmed by transthoracic echocardiography. The LV-volume-time functions of all volunteers are displayed in Figure 3 (left side, solid line). Individual parameters are given in Table 1.

### Cardiac MRE

Figure 2 shows phase signal oscillations in the RO direction spatially averaged within the semi-automatically derived ROI in the left ventricle. The boundaries of the ROI roughly indicate the area where the amplitude ratio  $U_{diastole}/$

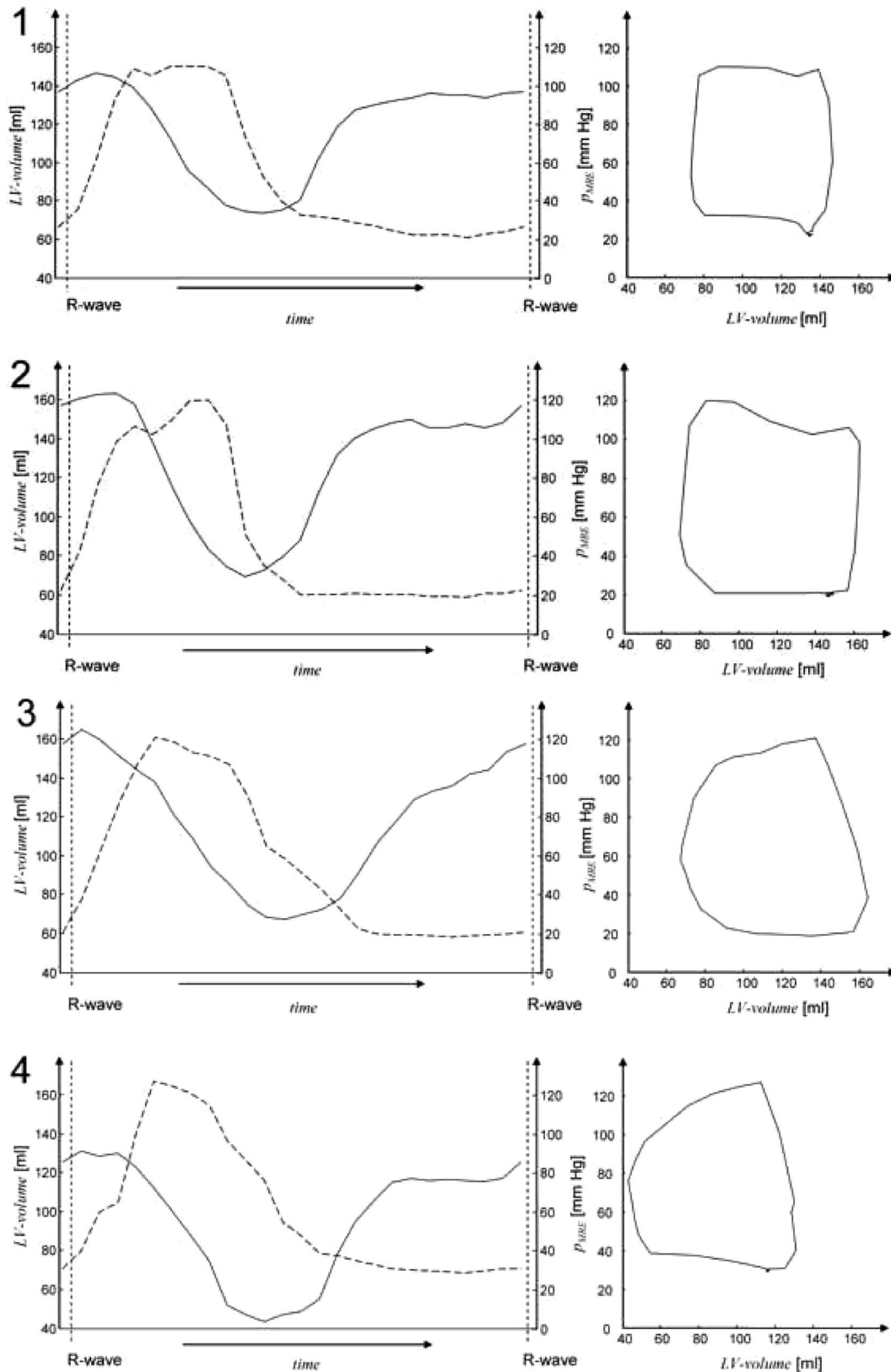


FIGURE 3. Volume-time functions (left side, solid line) and left ventricular wall pressure- time-function (left side, dashed line) from 8 volunteers (numbered 1–8) are plotted over one complete cardiac cycle (R-wave-R-wave). On the right side the resulting wall-pressure- volume cycles are displayed.

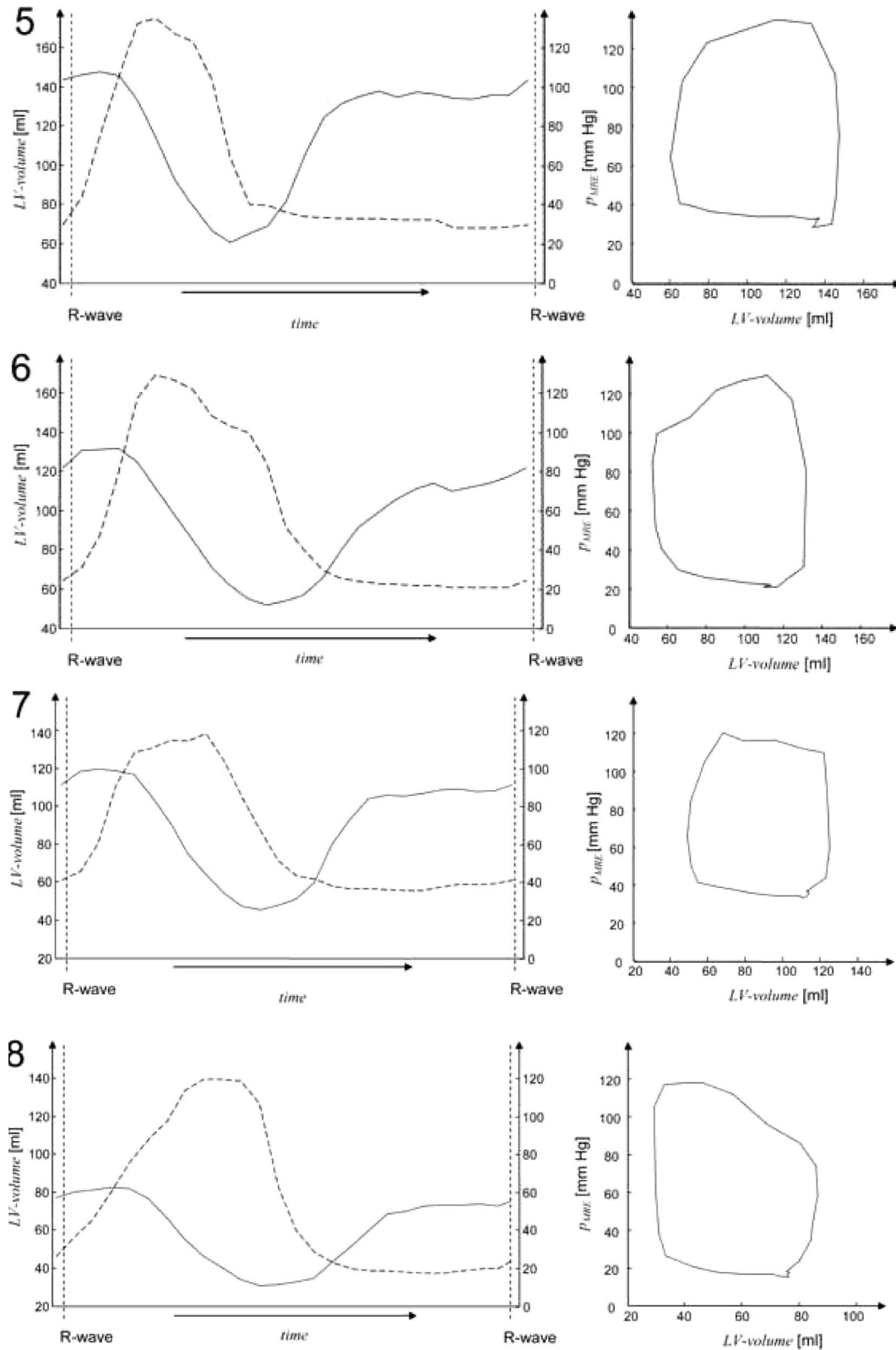


FIGURE 3. (continued).

**TABLE 1.** Global Corporal Parameters and Left Ventricular (LV) Data

Subject Number	Corporal Parameters			LV Parameters			
	Height (cm)	Body Weight (kg)	pRR (mm Hg)	EDV (ml)	EF (%)	MM (g)	RR-Interval (ms)
1a	173	74	130/64	147	50	116	1080
1b		72	120/73	129	55	108	1029
1c		72	120/62	123	59	114	888
2a	183	80	110/60	172	58	107	1092
2b		79	103/62	153	55	115	1001
2c		79	104/61	148	57	121	1049
3	183	85	120/70	165	59	127	748
4	193	75	130/80	111	61	102	970
5	190	90	135/70	147	59	120	1070
6	183	72	130/73	132	61	116	872
7 (Female)	175	62	118/69	120	60	96	870
8 (Female)	163	50	116/65	81	62	74	778
Mean	180.4	74.2	121/67	135.7	58.0	109.7	953
SD	9.7	10.4	10/6	25.1	3.6	14.1	119

Subjects are numbered from 1 to 8 (female, 7+8), interindividual data are shown through index a–c. Blood pressures according to the method of Riva Rocci (pRR). Global cardiac parameters as obtained from 3-D volumetry of the left ventricle: Enddiastolic volume (EDV), ejection fraction (EF) left ventricular myocardial mass (MM) and heart rate as RR-Interval.

$U_{systole} > 1$ . The small area in the posterior part of the heart was automatically excluded from the ROI and shows no or negative amplitude variations, presumably as an effect of the large distance to the driver and thus smaller wave amplitudes in combination with motion interference at the LV boundary and papillary muscles. Similar effects were seen in other volunteers mainly in regions where wave intensity is altered by noise resulting from intrinsic heart motions. The averaged motion data of the ROI are shown on the right hand side of Figure 2. The data clearly suggests that the wave amplitudes are higher during diastole than systole. Figure 3 (left column) shows  $p_{MRE}(t)$  and  $V(t)$  data on the time scale  $t$  of 1 R-R interval. Comparison of both functions reveals that  $p_{MRE}(t)$  precedes volume changes at the beginning of systole. This is similar to myocardial relaxation at the onset of diastole, where the change in volume also seems to follow the pressure drop. It was noted that the wave amplitudes start to decline about  $75 \pm 9$  milliseconds before the volume changes while their increase precedes heart motion by about  $159 \pm 23$  milliseconds (interindividual mean  $\pm$  SD). These delays strongly indicate the occurrence of IVC and IVR although their numbers are not comparable to invasive isovolumetric times. Quantification of the lengths of IVC and IVR by our data is limited because of the reduced time resolution of approximately 40 milliseconds. A better representation of the conservation of LV volume during pressure variation is obtained by plotting the  $p(V)$  function as shown by the P-V cycles in Figure 3 (right column). Note that  $p_{MRE}$  increases without major volume changes during early systole. A clear exception is observed in volunteer #3 who has an unusually low IVC pressure derivative  $p'_{IVC}$  of 3.8 mm Hg/ml. The mean  $p'_{IVC}$  averaged over the subjects excluding volunteer #3 is  $12.1 \pm 2.0$  mm Hg/ml. A larger interindividual variation was observed for the corresponding IVR-value ( $p'_{IVR} = 11.4 \pm 5.5$  mm Hg/ml), which indicates that most of the P-V cycles shown display a more pronounced volume conservation dur-

ing IVC than during IVR. The P-V work performed within one heart beat could be calculated from the enclosed area of the cycles. The standard deviation of all work data is approximately 13%, which is similar to that of the EDV data while  $\bar{p}_{systole}$  varies by about 8% among all volunteers. Thus, a major proportion of the variability of P-V data arises from LV volume differences among healthy subjects and not from MRE-relevant parameters. Individual and mean MRE-derived parameters are listed in Table 2.

## DISCUSSION

This study has demonstrated for the first time that it is feasible to perform cardiac elastography using shear waves for measuring pressure-related LV function parameters. The pressure measured by MRE,  $p_{MRE}$ , is similar to invasively determined LV-pressures reported in the literature in that it increases during IVC and decreases during IVR before the corresponding ventricular volume changes are observable by MRI. This is the most intriguing result of our study since it underscores that cardiac MRE is capable of measuring a new parameter, which cannot be determined by standard imaging modalities. Since the wave amplitudes clearly decline before the systolic and diastolic changes in LV volume start, we conclude that heart motion does not trigger the amplitude effect. Instead, the observed amplitude variation is caused by an effect that induces the heart to contract and to relax. Regardless of the physical nature of this effect, it can be perceived as a principal heart function compared with the morphologic changes of the heart that follow the shown amplitude curves.

The relationship between wave amplitudes and pressure remains a subject of research. The model developed in this study specifically applies to shear-wave-based elastography. The focus on pure shear deformation is justified by the high Lamé coefficient  $\lambda$  in soft biologic tissue which is up to 3 orders of magnitude larger than the shear modulus. Therefore,

TABLE 2. Parameters of Heart Function Measured by MRE

Subject Number	$ Az\bar{p}_{\text{systole}} $ (mm Hg)	SD	$ Az\bar{p}_{\text{diastole}} $ (mm Hg)	SD	$\Delta p$ (mm Hg)	$p'_{\text{IVC}}$ (mm Hg/ml)	$p'_{\text{IVR}}$ (mm Hg/ml)	W (J)
1a	108.4	1.5	24.4	3.4	84.2	11.4	17.6	0.73
1b	113.2	5	16.0	2.8	97.2	13.9	7.4	0.80
1c	105.3	7.6	13.9	0.8	91.4	13.8	7.6	0.79
2a	102.4	7.8	18.7	0.7	83.7	12.6	18.9	0.92
2b	92.8	13.6	18.8	2.7	74.0	11.5	8.7	0.73
2c	102.6	3.7	32.3	1.6	70.3	16.1	17.0	0.71
3	114.1	5.6	22.5	6.2	91.6	(3.8)	6.5	1.00
4	117.7	10.7	32.1	3.3	85.6	10.3	10.0	0.84
5	117.7	10.7	32.1	3.3	93.9	10.3	8.4	1.00
6	120.9	8.4	23.2	2.2	91.9	11.5	18.9	0.93
7 (Female)	112.2	6.9	19.1	1.5	93.1	12.0	8.8	0.78
8 (Female)	113.1	4	21.1	5.8	92	17.1	8.1	0.46
Mean	110.1	8.3	21.4	2.7	89.0	12.1	11.4	0.84
SD	7.7	5.5	8.1	1.8	9.7	2.0	5.5	0.19

Levels of iso-pressure  $|Az\bar{p}_{\text{systole}}|$  and  $|Az\bar{p}_{\text{diastole}}|$  with standard deviation (SD), pressure difference  $\Delta p = |Az\bar{p}_{\text{systole}}| - |Az\bar{p}_{\text{diastole}}|$ , pressure rise ( $p'_{\text{IVC}}$ ) and pressure drop ( $p'_{\text{IVR}}$ ) while volume conservation, cardiac stroke work W. See text for details.

in a low dynamic range, longitudinal tissue strain approaches very small amplitudes about 6 orders of magnitude smaller than the values of the shear strain.<sup>26</sup> In this respect, the investigation of the ventricular pressure by MRE requires a convergent elasticity model that avoids a nearly singular compression modulus and takes into account principal geometrical features of the left ventricle. The shear-displacement field in spherical coordinates developed by our group is a simple starting point for the evaluation of  $U(t)$  with respect to cavity pressure. Other forms of spherical divergence-free displacements yield radial stress components whose angular dependence may vary from our model. As long as a linear proportionality is assumed between shear modulus and cavity pressure we can use the myocardial shear modulus as a probe of ventricular pressure evolution according to Eq. 6. The externally measured blood pressure provides only a coarse approximation of the systolic LV pressure as it is influenced by the vascular resistance. Because of reflections, the peripheral blood pressure is higher than the maximal systolic LV pressure.<sup>27</sup> Nevertheless, this additional information maps the experimental shear modulus ratios onto a pressure scale and thus increases the comparability among individuals.

All 8 volunteers felt comfortable during the MRE examinations. None reported discomfort from mechanical actuation. The induced vibrations were perceived as a moderate buzz comparable to vibrations of a mowing machine. The noise level of the wave source was far below that of the imaging gradients. In general, low-frequency acoustic vibrations seem to feel more comfortable than other (interventional) techniques that can be used to assess ventricular pressure.

During the last years, few ultrasound studies have addressed myocardial elastography using the inherent contractile function of the heart as the mechanical stimulus.<sup>28,29</sup> Kanai<sup>30</sup> measured viscoelastic values of the myocardium ( $\mu = 24$  to 30 kPa) by exploiting the wall vibrations that occur

after aortic valve closure. Rump et al<sup>31</sup> used externally induced shear waves in MRI to derive preliminary elastic parameters between 5 and 27 kPa at 4 time points during the cardiac cycle. In contrast, the evaluation of wave amplitudes as shown in this study focuses on the dynamics of relative elasticity changes, which are hard to compare with absolute elasticity values measured at single<sup>30</sup> or very few time points.<sup>31</sup> Recently, Hsu et al<sup>32</sup> have used acoustic radiation force imaging on an exposed canine heart to analyze tissue displacement with respect to myocardial stiffness changes. They measured a stiffness ratio of 5.3:1 from systolic and diastolic displacements in the vicinity of the focus of the radiation force pulse. The mean ratio  $\bar{p}_{\text{systole}}/\bar{p}_{\text{diastole}}$  found in our study was  $5.1 \pm 1.3$  which is in good agreement with their value. However, the mean stiffness ratio is considerable smaller than the invasively measured factor of  $33 \pm 11$  in male control subjects.<sup>33,34</sup> As mentioned by Hsu et al,<sup>32</sup> the degree of relative displacement differences between systole and diastole is uncertain as the total deflection influences the observed amplitude variation. This uncertainty has not been addressed in our study since  $p_{\text{MRE}}$  was averaged over most of the LV area including myocardium and adjacent blood pool. Using the threshold  $U_{\text{diastole}}/U_{\text{systole}} > 1$  for ROI selection yielded the highest reproducibility with low noise in the  $U(t)$  data and high individual consistency. It remains to be determined in future investigations how significantly  $p_{\text{MRE}}$  varies locally. In the present study, our focus was on P-V characteristics with special attention to the IVC and IVR pressure change. Figure 3 demonstrates the expected IVC pressure rise in all volunteers except for volunteer #3. In this volunteer, the small  $p'_{\text{IVC}}$  value indicates an increased volume change during pressure increase. This volunteer was found to have mild mitral valve insufficiency, which explains the different  $p'_{\text{IVC}}$  value in this volunteer and shows an intriguing agreement between MRE and cardiac abnormality. However, as this diagnosis was a coincidental finding further data have to

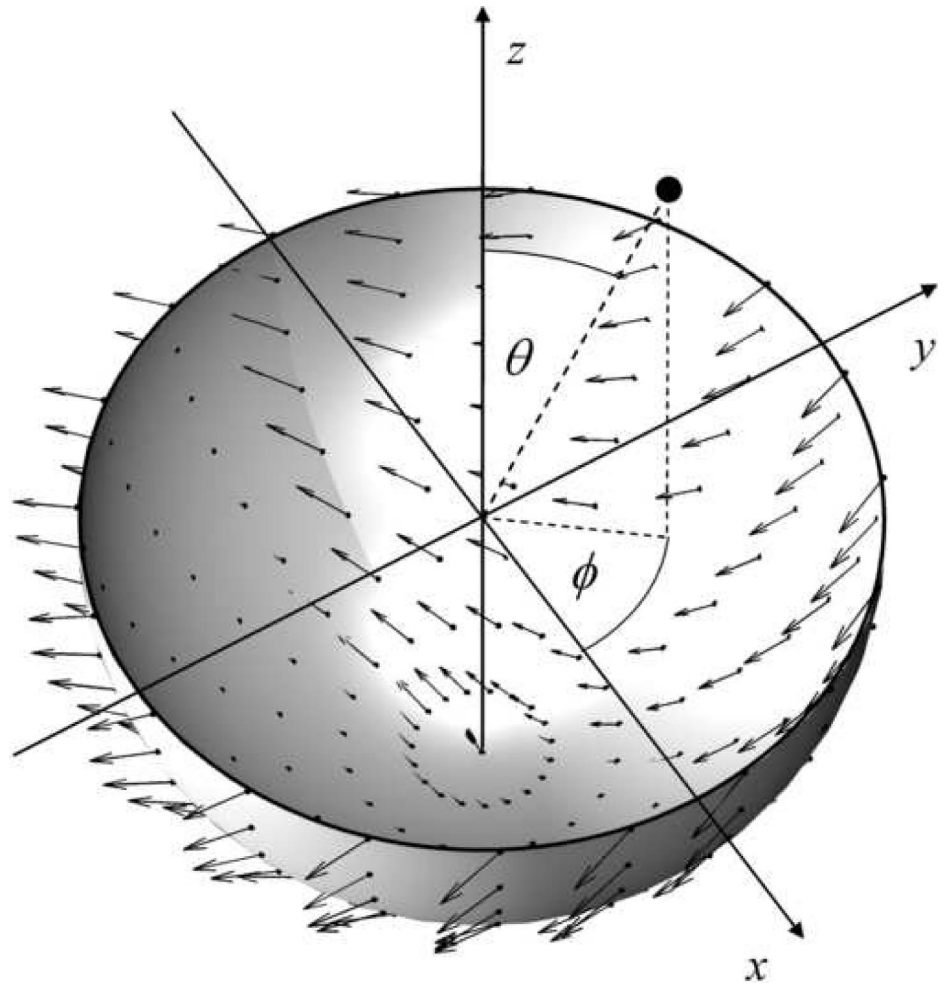


**FIGURE 4.** Polar angles and quiver representation of the compression-free displacement field on the surface of a half-sphere given in Eq. 3. A cavity pressure is generated due to radial stress components caused by the shear field.

be acquired to investigate the clinical significance of the  $p'_{IVC}$  parameter. Compared with the IVC branch, diastolic relaxation varies to a greater extent throughout all experiments. This variability in our volunteers may be because of various factors such as a physiologically different rate and extent of myocardial relaxation, geometrical and elastic myocardial properties, ventricular interaction and visco- or hyperelastic behavior.<sup>3,35</sup> The higher end-diastolic myocardial wall pressure compared with invasive measurements is most likely caused by myocardial pretension as a result of nonlinear effects.<sup>36</sup> Compared with ex vivo data from the literature (resting tension of  $3.5 \pm 1.7$  kPa in isolated myocytes from normal human heart biopsies)<sup>37</sup> the  $\bar{p}_{diastole}$ -values we measured ( $21.4 \pm 8.1$  mm Hg are equivalent to  $2.9 \pm 1.1$  kPa) correlate reasonable well. The P- V work we deduced from the MRE data ( $0.84 \pm 0.19$  J) is in the range reported in the literature ( $0.62 \pm 0.138$  J in normal subjects)<sup>38</sup> to ( $1.0 \pm 0.21$  J)<sup>39</sup> in patients with cardiac pathology and reduced EF). It has to be noted that the values for cardiac work strongly depend on ventricular volumes and blood pressure, giving rise to significant intra- and interindividual variations (Tables 1 and 2). In this respect, the correlation of cardiac MRE with LV-volumes and peripheral pressures remains to be determined. The repetition of the experiments of volunteers 1 and

2 are just a first step towards a full assessment of the reproducibility and the significance of cardiac MRE.

### Limitations

In this study, only a small number of healthy volunteers were examined, in whom direct comparison of this new method with invasive pressure measurements was not appropriate. A correlation of  $p_{MRE}$  and LV-pressure needs to be validated by interventions. The MRE measurements were obtained over a period of 2–3 minutes so that the resulting MRE pressure calculations reflect the average over this period of time. A different heart rate at the time of volume measurement and MRE could have distorted the values obtained. Under the controlled rest conditions in the volunteers, only minor changes in heart rate and blood pressure were observed during the examinations.

In summary, in vivo cardiac MRE is a noninvasive method for measuring myocardial shear modulus variations in terms of externally induced shear waves. The dynamics of the shear modulus in combination with LV volume changes reflect fundamental characteristics of ventricular pressure evolution such as pronounced IVC and IVR phases. Combined with MRI volumetry, cardiac MRE provides all parameters of heart function conveyed by a P-V cycle. This feasi-

bility study represents the first noninvasive mechanical testing of cardiac work in the human heart. Future studies will focus on the correlation with invasive pressure measurements and the significance of MRE-derived parameters for the diagnosis of specific cardiac dysfunctions.

**APPENDIX**

Here, a model is introduced to relate MRE wave amplitude data  $U(t)$  to LV pressure  $p(t)$ . The model assumes a spherical geometry of the ventricle and that the system is closed such that the free energy of the heart is a function of small deformations in the extension of linear elasticity theory. This assumption applies to the isovolumetric phases of the cardiac cycle when the ventricular valves are closed. In this way, the rise in ventricular pressure during IVC can be interpreted as the instantaneous pressure response to the increase in myocardial stiffness and small (isometric) deformations. Volume conservation holds due to the low compressibility of the myocardium and the blood. As a consequence, the assumed deformation field represents pure shear including any deviatoric deformation. In the following such shear field ( $\mathbf{u}$ ) is searched for deducing the radial stress component able to generate a pressure. Fields are given with respect to the unit vectors  $\mathbf{e}_r$ ,  $\mathbf{e}_\theta$  and  $\mathbf{e}_\phi$  in spherical coordinates  $r$ ,  $\theta$  and  $\phi$  (for definition, see Fig. 4). For simplicity, the radial dependence of both circumferential displacement components  $u_\theta$  and  $u_\phi$  shall be linear with  $\alpha r$ , where  $\alpha$  represents a small displacement angle. Using this dependence and employing the symmetry of the divergence operator (Div) in spherical coordinates, the following ansatz is made:

$$\mathbf{u} = u_r(r, \theta, \phi)\mathbf{e}_r + \alpha r \sin \theta \mathbf{e}_\theta + \alpha r \sin \theta \cos \phi \mathbf{e}_\phi \quad (2)$$

$u_r(r, \theta, \phi)$  is determined by solving  $\text{Div}(\mathbf{u}) = 0$ , which ensures that any compressional term in the resulting field is omitted. The  $\sin \theta$  terms in Eq. 2 prevent singularities  $u_r$  at  $\theta = 0$  while  $\cos \phi$  in  $u_\phi$  is chosen as an arbitrary function of  $\phi$  periodic with  $2\pi$ . Both conditions are important to ensure that the divergence-free displacement field is continuous over the entire space:

$$\mathbf{u} = \left( \frac{1}{3} \alpha r (\sin \phi - 2 \cos \theta) + \frac{C(\theta, \phi)}{r^2} \right) \mathbf{e}_r + \alpha r \sin \theta \mathbf{e}_\theta + \alpha r \sin \theta \cos \phi \mathbf{e}_\phi \quad (3)$$

As  $C(\theta, \phi)$  can be chosen arbitrarily it is considered to be zero. A 3D-surface projection of the field on a half-sphere shell is displayed in Figure 4. The Lagrange strain components of  $\mathbf{u}$  result with:

$$\begin{aligned} \varepsilon_{rr} &= \frac{1}{3} \alpha (\sin \phi - 2 \cos \theta); \quad \varepsilon_{\theta\theta} = \frac{1}{3} \alpha (\cos \theta + \sin \phi); \\ \varepsilon_{\phi\phi} &= \frac{1}{3} \alpha (\cos \theta - 2 \sin \phi) \quad \varepsilon_{r\theta} = \frac{1}{3} \alpha \sin \theta; \\ \varepsilon_{\theta\phi} &= 0; \quad \varepsilon_{r\phi} = \frac{1}{6} \frac{\alpha \cos \phi}{\sin \theta} \end{aligned} \quad (4)$$

The trace of the strain tensor  $\varepsilon$  is essentially zero and  $\varepsilon$  does not depend on  $r$  based on our assumptions. The equilibrium of forces is given with consideration of a cavity pressure  $p$  and the radial shear stress component  $\sigma_{rr}$ :

$$pS_r = 2 \int_{S_r} \sigma_{rr} dS_r; \quad \sigma_{rr} = 2\mu\varepsilon_{rr} \quad (5)$$

$S_r$  denotes the surface of an infinitesimal-thin spherical-shell with aperture. Such an opening mimics regions without muscle in the LV boundaries as they are present at the valvular sites. No stress is produced at these sites and as a result, a net pressure force  $pS_r$  is obtained whose value depends on the position and the size of the aperture. For example, assuming a half-sphere with  $\phi = 0..2\pi$  and  $\theta = 0.. \pi/2$  yields  $P = -3/4\alpha\mu$ . Depending on the aperture size  $p$  ranges from  $-8/3\alpha\mu$  to zero for the integration boundaries of  $\theta = 0$  to  $\theta = 0.. \pi$ , respectively. In general,  $P = -A\alpha\mu$  with  $A$  being a constant that depends on the geometrical settings of the model. Assuming that  $\alpha$  is solely determined by the contractile properties of the myocardium and not by  $\mu$ , we further draw  $\alpha$  into the geometrical constant  $A$  leading to

$$\frac{\mu(t_1)}{\mu(t_2)} = \frac{p(t_1)}{p(t_2)} \quad (6)$$

$t_1$  and  $t_2$  represent different time points during the cardiac cycle. In cardiac MRE  $\mu(t_1)$  and  $\mu(t_2)$  are measured by the wave amplitudes  $U(t_1)$  and  $U(t_2)$ . A relationship between  $\mu(t)$  and  $U(t)$  can readily be derived from the energy balance in a material subjected to harmonic shear vibrations. The imposed flow of oscillating energy density through unit surface is given by the intensity of the waves or the so-called flux<sup>20</sup>:

$$\langle F \rangle = \frac{1}{2} \rho c(t) U(t)^2 \omega^2 = const. \quad (7)$$

$\omega$  is the angular driving frequency of the waves,  $\rho$  is the density of the material and  $c(t)$  denotes the time variable shear wave speed in the myocardium ( $c = \sqrt{\mu/\rho}$ ). Constant wave intensity is gained by considering the expectation value of  $F$  over a wave period indicated by the brackets. Combining Eqs. 6 and 7 leads to Eq. 1 if  $t_2$  is assigned to the time of the systole.

**ACKNOWLEDGMENTS**

The authors thank Dr. Adrian-Constantin Borges for his support with echocardiography.

**REFERENCES**

- Magorien DJ, Shaffer P, Bush CA, et al. Assessment of left ventricular pressure- volume relations using gated radionuclide angiography, echocardiography, and micromanometer pressure recordings. A new method for serial measurements of systolic and diastolic function in man. *Circulation*. 1983;67:844–853.
- Covell JW, Ross J Jr, Sonnenblick EH, et al. Comparison of the

- force-velocity relation and the ventricular function curve as measures of the contractile state of the intact heart. *Circ Res.* 1966;19:364–372.
3. Burkhoff D, Mirsky I, Suga H. Assessment of systolic and diastolic ventricular properties via pressure-volume analysis: a guide for clinical, translational, and basic researchers. *Am J Physiol Heart Circ Physiol.* 2005;289:H501–H512.
  4. Kass DA. Assessment of diastolic dysfunction. Invasive modalities. *Cardiol Clin.* 2000;18:571–586.
  5. Stolzmann P, Scheffel H, Trindade PT, et al. Left ventricular and left atrial dimensions and volumes: comparison between dual-source CT and echocardiography. *Invest Radiol.* 2008;43:284–289.
  6. Mewton N, Croisille P, Revel D, et al. Left ventricular postmyocardial infarction remodeling studied by combining MR-tagging with delayed MR contrast enhancement. *Invest Radiol.* 2008;43:219–228.
  7. Hosch W, Bock M, Libicher M, et al. MR-relaxometry of myocardial tissue: significant elevation of T1 and T2 relaxation times in cardiac amyloidosis. *Invest Radiol.* 2007;42:636–642.
  8. Oh JK, Hatle L, Tajik AJ, et al. Diastolic heart failure can be diagnosed by comprehensive two-dimensional and Doppler echocardiography. *J Am Coll Cardiol.* 2006;47:500–506.
  9. Kasner M, Westermann D, Steendijk P, et al. Utility of Doppler echocardiography and tissue Doppler imaging in the estimation of diastolic function in heart failure with normal ejection fraction: a comparative Doppler-conductance catheterization study. *Circulation.* 2007;116:637–647.
  10. Parker KJ, Huang SR, Musulin RA, et al. Tissue response to mechanical vibrations for “sonoelasticity imaging”. *Ultrasound Med Biol.* 1990;16:241–246.
  11. Muthupillai R, Lomas DJ, Rossman PJ, et al. Magnetic resonance elastography by direct visualization of propagating acoustic strain waves. *Science.* 1995;269:1854–1857.
  12. Fung Y. *Biomechanics: Mechanical Properties of Living Tissue.* New York: Springer-Verlag; 1993.
  13. Huwart L, Sempoux C, Salameh N, et al. Liver fibrosis: noninvasive assessment with MR elastography versus aspartate aminotransferase-to-platelet ratio index. *Radiology.* 2007;245:458–466.
  14. Yin M, Talwalkar JA, Glaser KJ, et al. Assessment of hepatic fibrosis with magnetic resonance elastography. *Clin Gastroenterol Hepatol.* 2007;5:1207–1213, e1202.
  15. Sack I, Beierbach B, Hamhaber U, et al. Non-invasive measurement of brain viscoelasticity using magnetic resonance elastography. *NMR Biomed.* 2008;21:265–271.
  16. Klatt D, Hamhaber U, Asbach P, et al. Noninvasive assessment of the rheological behavior of human organs using multifrequency MR elastography: a study of brain and liver viscoelasticity. *Phys Med Biol.* 2007;52:7281–7294.
  17. Manduca A, Lake DS, Kruse SA, et al. Spatio-temporal directional filtering for improved inversion of MR elastography images. *Med Image Anal.* 2003;7:465–473.
  18. Park E, Maniatty AM. Shear modulus reconstruction in dynamic elastography: time harmonic case. *Phys Med Biol.* 2006;51:3697–3721.
  19. Sinkus R, Siegmann K, Xydeas T, et al. MR elastography of breast lesions: Understanding the solid/liquid duality can improve the specificity of contrast-enhanced MR mammography. *Magn Reson Med.* 2007;58:1135–1144.
  20. Achenbach JD. *Wave Propagation in Elastic Solids.* Amsterdam: Elsevier; 1999.
  21. Mirsky I, Pasipoularides A. Clinical assessment of diastolic function. *Prog Cardiovasc Dis.* 1990;32:291–318.
  22. Sack I, Rump J, Elgeti T, et al. MR elastography of the human heart: Noninvasive assessment of myocardial elasticity changes by shear wave amplitude variations. *Magn Reson Med.* 2008;in revision.
  23. Klatt D, Asbach P, Rump J, et al. In vivo determination of hepatic stiffness using steady-state free precession magnetic resonance elastography. *Invest Radiol.* 2006;41:841–848.
  24. Woodrum DA, Romano AJ, Lerman A, et al. Vascular wall elasticity measurement by magnetic resonance imaging. *Magn Reson Med.* 2006;56:593–600.
  25. Alfakih K, Plein S, Thiele H, et al. Normal human left and right ventricular dimensions for MRI as assessed by turbo gradient echo and steady-state free precession imaging sequences. *J Magn Reson Imaging.* 2003;17:323–329.
  26. Aki K, Richards PG. *Quantitative Seismology.* Sausalito: University Science Books; 2002.
  27. Elzinga G, Westerhof N. Pressure and flow generated by the left ventricle against different impedances. *Circ Res.* 1973;32:178–186.
  28. Konofagou EE, D’Hooge J, Ophir J. Myocardial elastography—a feasibility study in vivo. *Ultrasound Med Biol.* 2002;28:475–482.
  29. Luo J, Fujikura K, Homma S, et al. Myocardial elastography at both high temporal and spatial resolution for the detection of infarcts. *Ultrasound Med Biol.* 2007;33:1206–1223.
  30. Kanai H. Propagation of spontaneously actuated pulsive vibration in human heart wall and in vivo viscoelasticity estimation. *IEEE Trans Ultrason Ferroelectr Freq Control.* 2005;52:1931–1942.
  31. Rump J, Klatt D, Braun J, et al. Fractional encoding of harmonic motions in MR elastography. *Magn Reson Med.* 2007;57:388–395.
  32. Hsu SJ, Bouchard RR, Dumont DM, et al. In vivo assessment of myocardial stiffness with acoustic radiation force impulse imaging. *Ultrasound Med Biol.* 2007;33:1706–1719.
  33. Hayward CS, Kalnins WV, Kelly RP. Gender-related differences in left ventricular chamber function. *Cardiovasc Res.* 2001;49:340–350.
  34. Zile MR, Baicu CF, Gaasch WH. Diastolic heart failure—abnormalities in active relaxation and passive stiffness of the left ventricle. *N Engl J Med.* 2004;350:1953–1959.
  35. Gilbert JC, Glantz SA. Determinants of left ventricular filling and of the diastolic pressure-volume relation. *Circ Res.* 1989;64:827–852.
  36. Kass DA, Bronzwaer JG, Paulus WJ. What mechanisms underlie diastolic dysfunction in heart failure? *Circ Res.* 2004;94:1533–1542.
  37. Borbely A, van der Velden J, Papp Z, et al. Cardiomyocyte stiffness in diastolic heart failure. *Circulation.* 2005;111:774–781.
  38. Alter P, Rupp H, Rominger MB, et al. A new methodological approach to assess cardiac work by pressure-volume and stress-length relations in patients with aortic valve stenosis and dilated cardiomyopathy. *Pflugers Arch.* 2008;455:627–636.
  39. Asanoi H, Kameyama T, Ishizaka S, et al. Energetically optimal left ventricular pressure for the failing human heart. *Circulation.* 1996;93:67–73.